No-reference evaluation of the reconstructed images in single-shot K-Edge Subtraction X-ray Computed Tomography

G. Saccomano[1], V. Di Trapani[2], P. Delogu[2] and F. Brun[1]
[1] *Dipartimento di Ingegneria e Architettura, Università degli Studi di Trieste, Trieste, Italy*
[2] *Dipartimento Scienze fisiche, della Terra e dell'ambiente, Università degli Studi di Siena, Siena, Italy*

***Abstract*—Single-shot K-Edge Subtraction X-ray Computed Tomography (CT) with a multi-threshold photon-counting detector is an interesting approach to favour low-dose analyses of a known contrast agent with promising applications *in vivo*. To assess the minimum detectable concentration of the contrast agent and to favour possible radiation dose reduction and/or faster acquisition time, a significant role is played by the tomographic reconstruction algorithm. By considering experimental images, this work evaluates three CT reconstruction methods and different acquisition statistics via a no-reference assessment of contrast-to-noise ratio and spatial resolution. The results support that, although computationally expensive, a SART-TV reconstruction approach yields adequate results even when a limited number of projections is available.**

***Keywords*—spectral imaging, photon counting detector, computed tomography, iterative reconstruction.**

I. Introduction

Within the field of X-ray spectral imaging [1], K-Edge Subtraction (KES) considers the sharp rise of the absorption coefficient at the K-edge of a specific element such as e.g. an injected contrast agent. This imaging technique requires the acquisition of two digital images at different energies at either side of the K-edge of the element to be detected and it can be applied to Computed Tomography (CT). The logarithmic subtraction of these "low" and "high" energy images enhances the presence of the element whereas the other structures have negligible (or negative) contrast, thus favoring further image segmentation and analysis.

KES imaging with conventional polychromatic sources is of great interest and it would be desirable to obtain the energy images in a *single shot* by separating the spectrum in (at least) two parts, i.e. below and above the K-edge of an element. An X-ray Photon Counting Detector (XPCD) is the most promising tool for single-shot KES imaging [2], since it is equipped with a real time multi-threshold discrimination system and it is therefore capable to acquire perfectly co-registered data over multiple energy bins in a single scan.

This work considers different reconstruction methods for X-ray KES CT images of Ba solutions. Experimental images acquired with the Pixie-III detector [3]–[6] are analyzed. This work aims at evaluating different KES CT reconstruction algorithms by proposing a simple no-reference quality evaluation method based on an assessment of contrast-to-noise ratio and spatial resolution directly from the reconstructed images. The ultimate goals of this work are: i) to investigate if refined iterative reconstruction algorithms for KES-CT allow to detect subtle concentrations of a contrast agent thanks to a better noise compensation and ii) to speculate about the reconstruction algorithm that, among the considered ones, better tolerates a projection decimation since this generally favors a radiation dose reduction and/or faster acquisition times.

II. Materials and Methods

A. Sample preparation

A test object composed of polypropylene 350 µl small tubes filled with different dilutions of $BaCl_2$ (Carlo Erba Reagents — 122 mg/ml) and de-ionized water was prepared. Fig. 1 depicts a sketch of this test object together with its setup with respect to the beam and the detector.

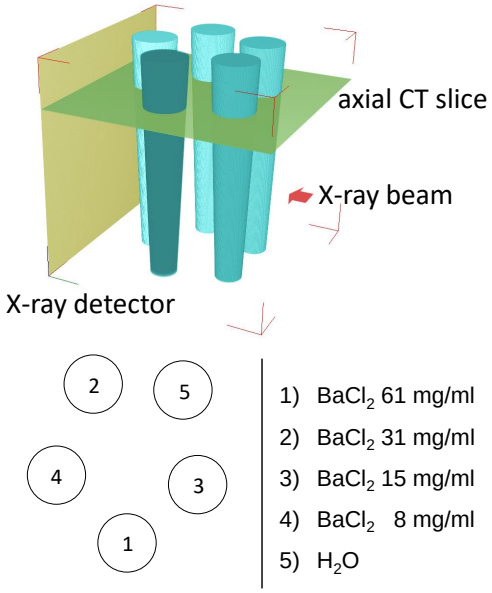

Fig. 1: Sketch of KES CT imaging setup (top panel) and the considered test object composed of different pipettes filled with a Ba solution with the order and composition as it results from an axial CT slice (bottom panel).

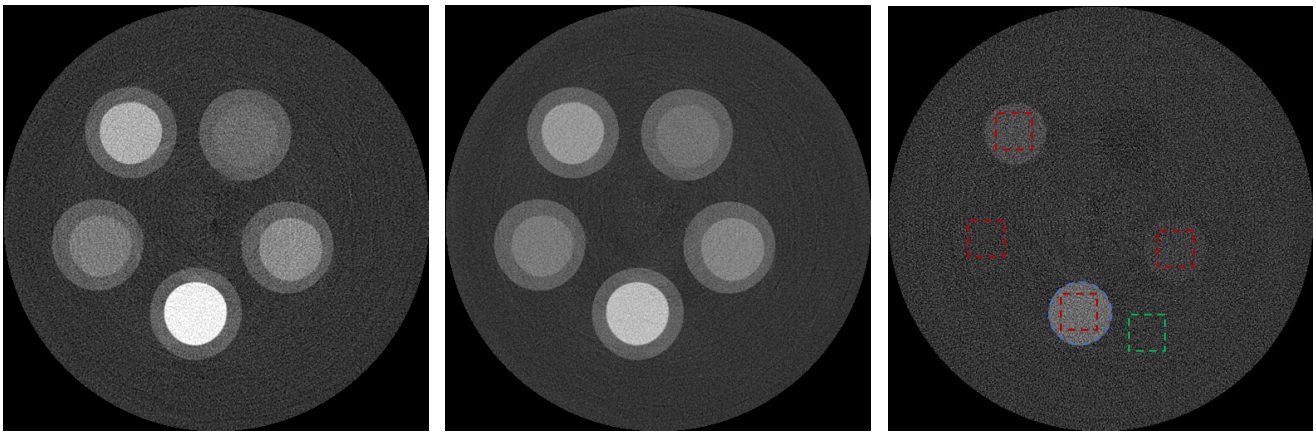

Fig. 2: CT axial slice (512×512 pixels) reconstructed with FDK of the considered test object: a) low-energy image; (b) high-energy image; c) resulting KES image where only the Ba content within the small tubes results highlighted. Resulting isotropic voxel size is 50×50×50 μm^3. The same window/level gray-value settings are used for the three images. The highlighted ROIs are used for quantitative analysis. [Scale bar = 5 mm]

B. CT acquisition

A micro-focus Hamamatsu X-ray source (tube voltage: 20 to 90 kV, tube current: 0 to 200 µA, maximum output: 8 W, focal spot size: 5 µm) and a CdTe Pixirad-1/Pixie-III detector (sensitive area: 31.7 25.0 mm^2 organized as a 512 402 pixels on a square matrix at 62 µm pitch) were used. The detector was configured in Neighbor Pixel Inhibit - Pixel Summing Mode (NPISUM) [5]. This mode is specifically designed to favor energy resolution [6].

Thanks to its two programmable energy thresholds E_{low} and E_{high}, the detector outputs in a single exposure two images, hereafter referred as to "low" (in the energy range [E_{low},E_{high}]) and "high" (in the range [E_{high},+ *1*]). Fig. 2 reports a sample slice of these "low", "high" and KES datasets.

For this work the following acquisition settings were used: X-ray tube voltage = 50 kV, current = 160 µA, 1mm Al filter, exposure time = 1 s, detector energy thresholds E_{low} = 28.0 keV, E_{high} = 38.0 keV. These settings result from the optimization reported in [7]. The cone-beam CT geometry setttings are: distance source-to-object D_{SO} = 200 mm, distance source-to-detector D_{SD} = 250 mm, 720 projections over 360 degrees in "step and go" mode. Projection averaging over 10 images was applied. The nominal voxel size of the reconstructed 512 512 axial slices is 50 50 50 μm^3.

C. Image pre-processing

In addition to conventional flat-fielding, a custom automatic detection and removal non-linear filter was used to compensate for a few observed defective pixels. This filter considers a 5 5 neighborhood and its median gray value m. If the absolute difference between the gray-level of the central pixel and m is above a user-specified fixed threshold , the value of the central pixel is then replaced. The replaced value is not m but it is the median of the set composed by the pixels that satisfy the previous condition, i.e. having the absolute difference between their gray level and m below the threshold.

D. Reconstruction algorithms

In this work the following reconstruction algorithms were considered: FDK, OS-SART, and SART-TV. The implementation available in the open-source software TIGRE was used [8]. Default parameters were considered for each algorithm except for the filtering of the FDK where "shepp-logan" was applied and for the parameter of SART-TV (= 500 was set). For the SART-based algorithms 200 iterations were applied. To simulate different acquisition statistics, projections were decimated in order to have three input datasets composed of 720, 360, and 180 projections, respectively. For each considered algorithm, a post-reconstruction ring-removal filter was applied directly to the reconstructed slices [9].

E. Quantitative analysis

The reconstructed images were quantitatively compared in terms of spatial resolution x and contrast-to-noise ratio CNR by considering the central slice of the reconstructed volume. The circular edge method with a logistic curve-fitting technique [10] was used to asses the spatial resolution as Full Width Half Maximum (FWHM) of the first derivative of the edge spread function. The circular edge reported in blue in Fig, 2 was considered. The Regions-of-Interests (ROIs) reported in red as well as reference ROI_0 highlighted in green in Fig, 2 were used to compute the mean and standard deviation of the gray levels. Then CNR for each ROI i-th was determined as:

$$CNR_i = \frac{j \quad _i \quad \quad _0 j}{\sqrt{(\ ^2_i + \ ^2_0)/2}}: \tag{1}$$

A simple quality characteristic Q defined as:

$$Q = \frac{CNR_1}{x} \tag{2}$$

is here proposed to combine CNR and spatial resolution information in a single metric.

TABLE I: Results of the quantitative analysis of CNR

Algorithm	CNR_1	CNR_2	CNR_3	CNR_4
FDK *j* 720	2.48	1.14	0.43	0.06
FDK *j* 360	1.66	0.76	0.29	0.03
FDK *j* 180	1.15	0.51	0.19	0.02
OS-SART *j* 720	1.19	0.54	0.24	0.05
OS-SART *j* 360	1.27	0.55	0.22	0.02
OS-SART *j* 180	1.59	0.71	0.26	0.01
SART-TV *j* 720	5.81	2.64	1.01	0.11
SART-TV *j* 360	6.18	3.04	1.10	0.12
SART-TV *j* 180	6.78	3.06	1.14	0.16

TABLE II: Results of the quantitative analysis of Δx and Q

Algorithm	x [mm]	Q [mm^{-1}]
FDK *j* 720	0.091	27.1
FDK *j* 360	0.089	18.7
FDK *j* 180	0.096	12.1
OS-SART *j* 720	0.077	15.4
OS-SART *j* 360	0.075	16.9
OS-SART *j* 180	0.134	11.9
SART-TV *j* 720	0.106	54.8
SART-TV *j* 360	0.126	49.0
SART-TV *j* 180	0.169	39.9

III. Results and discussion

Table I reports the quantitative results of the assessment of CNR for each considered Ba dilutions. It can be noticed that although the pipette filled with the minimum concentration of Ba results hard to detect for all the considered algorithms, an interesting difference is observed for the pipette filled with 15 mg/ml of $BaCl_2$. The images reconstructed with SART-TV present a value for CNR_3 above 1 for each considered projection decimation. It is worthy to note also that CNR values for the FDK images decrease when reducing the number of available projections. This is not true for the SART-based algorithms where a better noise handling with a consequently smoothing effect results in increasing CNR values for ROI_1 and ROI_2. These results support that SART-TV allow to detect a subtle concentrations of the contrast agent thanks to its better noise compensation even when a limited number of projections is available.

Because higher values for CNR might be related to a worsening of the spatial resolution, the previous observation needs to take into account the quantitative results for x and Q reported in Table II. It can be observed that for FDK the value of Q increases coherently when more projections are available. This observation does not hold for OS-SART. Interestingly, the highest value of Q for OS-SART is recorded for the case considering 360 projections, thus suggesting that 720 projections are not necessary for the reconstruction of a 512 512 image with this algorithm. While the assessed spatial resolution for FDK is superior to the one for the SART-TV case, the assessed x values for SART-TV might be acceptable for an experimental voxel size of 50 50 50 μm^3.

The computed quality measurements still support the use of FDK when a high number of projections are collected, especially for applications in which spatial resolution has to be privileged. However, the loss in x for SART-TV might be tolerated for practical applications where the detectability of subtle concentrations has to be favored. Moreover, although a more refined and detailed investigation is required, the parameter of SART-TV seems to act as a trade-off between these two aspects, thus allowing an application-dependent fine tuning of the final quality of the reconstructed images. This option is not available for the FDK algorithm.

Computational requirements are of course different for the three considered algorithms, being FDK the fastest reconstruction approach and SART-TV the most computationally intense. Refined investigations are required to optimize the number of iterations required by the SART-based techniques. It is reasonable to assume that 200 iterations as considered in this work are more than abundant for the vast majority of the applications. A convergence analysis is required to optimize the computational aspects of a SART-based reconstruction workflow.

References

[1] E. Fredenberg, "Spectral and dual-energy X-ray imaging for medical applications," *Nuclear Instruments and Methods in Physics Research, Section A: Accelerators, Spectrometers, Detectors and Associated Equipment*, vol. 878, pp. 74–87, 2018.

[2] J. Schlomka, E. Roessl, R. Dorscheid, S. Dill, G. Martens, T. Istel, and et al., "Experimental feasibility of multi-energy photon-counting k-edge imaging in pre-clinical computed tomography," *Physics in Medicine and Biology*, vol. 53, no. 15, pp. 4031–4047, 2008.

[3] F. Brun, V. Di Trapani, D. Dreossi, R. Longo, P. Delogu, and L. Rigon, "K-edge spectral computed tomography with a photon counting detector and discrete reconstruction," *Annual International Conference of the IEEE Engineering in Medicine and Biology Society*, vol. 2018, pp. 5245–5248, 2018.

[4] F. Brun, V. Di Trapani, D. Dreossi, L. Rigon, R. Longo, and P. Delogu, "Towards in vivo K-edge X-ray micro-CT with the Pixirad-I/Pixie-III detector," *IFMBE Proceedings*, vol. 68, no. 1, pp. 123–126, 2019.

[5] V. Di Trapani, A. Bravin, F. Brun, D. Dreossi, R. Longo, A. Mittone, and et al., "Characterization of noise and efficiency of the pixirad-1/pixie-III CdTe x-ray imaging detector," *Journal of Instrumentation*, vol. 13, pp. C12008–C12008, dec 2018.

[6] V. Di Trapani, A. Bravin, F. Brun, D. Dreossi, R. Longo, A. Mittone, and et al., "Characterization of the acquisition modes implemented in Pixirad-1/Pixie-III X-ray Detector: Effects of charge sharing correction on spectral resolution and image quality," *Nuclear Instruments and Methods in Physics Research, Section A: Accelerators, Spectrometers, Detectors and Associated Equipment*, vol. 955, p. 163220, 2020.

[7] F. Brun, V. D. Trapani, J. Albers, P. Sacco, D. Dreossi, L. Brombal, and et al., "Single-shot K-Edge subtraction X-ray discrete computed tomography with a polychromatic source and the Pixie-III detector," *Physics in Medicine Biology*, 2020, published on-line DOI:10.1088/1361-6560/ab7105.

[8] A. Biguri, M. Dosanjh, S. Hancock, and M. Soleimani, "TIGRE: A MATLAB-GPU toolbox for CBCT image reconstruction," *Biomedical Physics and Engineering Express*, vol. 2, no. 5, 2016.

[9] F. Brun, A. Accardo, G. Kourousias, D. Dreossi, and R. Pugliese, "Effective implementation of ring artifacts removal filters for synchrotron radiation microtomographic images," *International Symposium on Image and Signal Processing and Analysis, ISPA*, pp. 672–676, 2013.

[10] T. Takenaga, S. Katsuragawa, M. Goto, M. Hatemura, Y. Uchiyama, and J. Shiraishi, "Modulation transfer function measurement of ct images by use of a circular edge method with a logistic curve-fitting technique," *Radiological Physics and Technology*, vol. 8, pp. 53–59, Jan 2015.

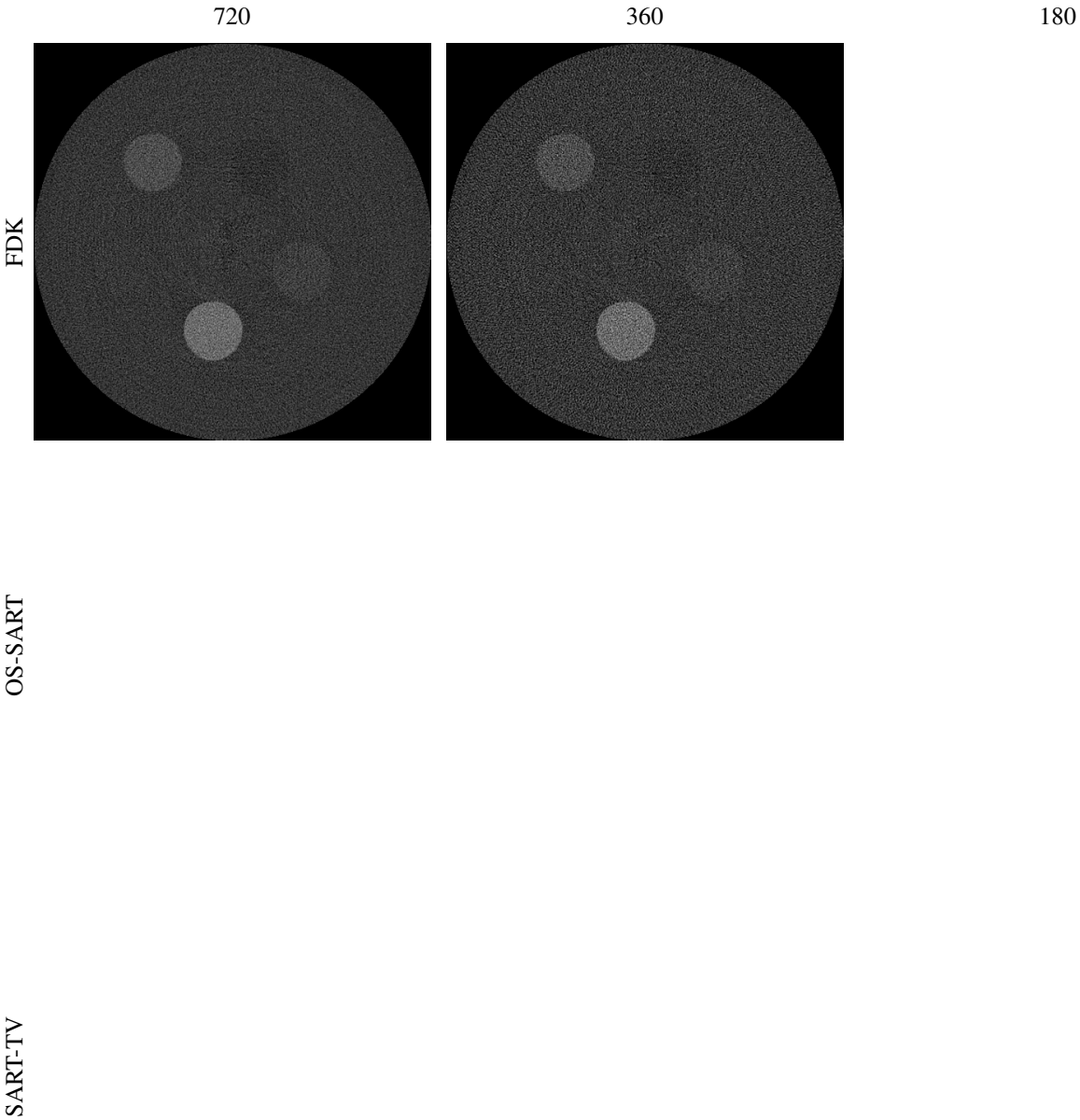

Fig. 3: A representative axial slice for each of the considered reconstruction algorithm and for the three different angular sampling (i.e. number of projections). From top to bottom: FDK, OS-SART, and SART-TV. From left to right: 720, 360, and 180 projections.